Elliptical orbits of microspheres in an evanescent field

Lulu Liu[a], Simon Kheifets[a], Vincent Ginis[a,b,1], Andrea Di Donato[a,c], and Federico Capasso[a,1]

[a]Harvard John A. Paulson School of Engineering and Applied Sciences, Harvard University, Cambridge, MA 02138; [b]Department of Physics, Vrije Universiteit Brussel, 1050 Brussels, Belgium; and [c]Dipartimento di Ingegneria dell'Informazione, Università Politecnica delle Marche, 60131 Ancona, Italy

Contributed by Federico Capasso, August 30, 2017 (sent for review January 6, 2017; reviewed by Vincent Daria and Kishan Dholakia)

We examine the motion of periodically driven and optically tweezed microspheres in fluid and find a rich variety of dynamic regimes. We demonstrate, in experiment and in theory, that mean particle motion in 2D is rarely parallel to the direction of the applied force and can even exhibit elliptical orbits with nonzero orbital angular momentum. The behavior is unique in that it depends neither on the nature of the microparticles nor that of the excitation; rather, angular momentum is introduced by the particle's interaction with the anisotropic fluid and optical trap environment. Overall, we find this motion to be highly tunable and predictable.

optical forces | colloids | microparticles | evanescent field | elliptical motion

Recently, much work has gone into the investigation of optical forces on micro- and nanoparticles near surfaces, primarily in the context of an electric field localized by a microstructured surface (1–5).

Surface-based geometries have raised theoretical excitement due to, for instance, their ability to significantly enhance optical forces (6–8) as well as the emergence of lateral forces due to the extraordinary momentum and spin in evanescent waves (9–12). From an applied point of view, such geometries can enable miniaturization and parallelization of efficient optical traps enabling integration into optofluidic devices (13, 14). Moreover, light-controlled microspheres near surfaces have found applications as force transducers (15–18) and pumps and switches (19, 20), and in general, their collective manipulation is an advancing field (21–23).

However, in the case where a microparticle is within several diameters of a surface, optical and hydrodynamic surface effects cannot be neglected. Effects arising from optical coupling or reflections can complicate trapping and detection schemes (24), and hydrodynamic interactions can cause the motion of a microparticle to become highly nontrivial (25). Despite this, little quantitative study has been done on the dynamics of optically driven particles near a surface. In studies introducing new schemes to optically manipulate matter, the particle's response function is often ignored (11, 12, 26–29).

In this work, we investigate the dynamics of a system with both near field optical forces and surface-induced hydrodynamic effects (see Fig. 1). By driving the particle with an oscillating force from a modulated evanescent field and tracking the particle's motion closely in two dimensions, we map out a range of dynamics that can arise from the interplay of optical and hydrodynamic surface effects. We find that the magnitude and direction of the optical force depends on particle size. We also observe that the trajectory of the particle in general does not follow the direction of the force. Instead, the shape and the orientation of the trajectory vary with modulation frequency and distance of the particle from the surface, a result of the anisotropy in both the hydrodynamic drag and the optical trap spring constant.

In particular, we find that under certain conditions, controlled, elliptical motion of a microsphere can be achieved in this configuration, without the use of a beam that carries either orbital or spin angular momentum. This motion is of theoretical and practical interest as it arises due to the particle's interaction with the inherently anisotropic mechanical environment nearby a solid interface as it moves in response to a periodic driving force. It has several distinguishing features that may make it an applicable technique for generating orbital angular momentum, alongside existing methods predominantly using structured beams carrying orbital or spin angular momentum (30–36). For a detailed discussion, please see *The Evanescent Wave Technique as a Method of Angular Momentum Generation*, following *Experiment*.

Forces on an Optically Driven and Trapped Microsphere

An optically trapped microsphere in fluid is well-modeled as a stochastically driven, damped harmonic oscillator in three dimensions (37, 38):

$$m^{\star}\ddot{x}_i(t) = -\kappa_{ij}x_j(t) - \gamma_{ij}\dot{x_j}(t) + B_i(t) + F_i(t). \qquad [1]$$

The terms on the right of Eq. **1** correspond, in order, to the restoring force of the optical trap, the dissipative drag in fluid, the stochastic force due to thermal fluctuations, and an externally applied force. Here, we apply a force and consider motion only in the two measured (x and z) dimensions.

Due to the symmetries in our system, the trap stiffness, κ_{ij}, is a diagonal tensor. For a single beam optical trap, its diagonal elements are not equal, $\kappa_x \neq \kappa_z$; that is, the harmonic potential is anisotropic. Usually, the magnitude of the spring constant in the lateral direction is several times larger than the spring constant in the axial direction (39). In our model describing the particle motion, we approximate that κ_i is a constant in z, an assumption that is generally valid until the separation becomes smaller than

Significance

Using a highly sensitive particle-tracking scheme, we report an observation of elliptical motion of microparticles driven by a single evanescent field. We show that this behavior is highly tunable and predictable using a theoretical model that accounts for Mie scattering and hydrodynamic drag. The significance is twofold. First, our work represents an important step in understanding the detailed dynamics of microparticles in a fluidic environment—especially near a surface—a prerequisite for effective application of optically driven microparticles as functional elements in optofluidic devices. Second, our method could complement current structured-light approaches for inducing orbital motion in microparticles, with readily tunable parameters of motion including orbital frequency, radius, and ellipticity.

Author contributions: L.L., S.K., V.G., and F.C. designed research; L.L., S.K., and A.D.D. performed research; F.C. oversaw research; L.L. and V.G. contributed new reagents/analytic tools; L.L., S.K., V.G., and A.D.D. analyzed data; and L.L., S.K., V.G., A.D.D., and F.C. wrote the paper.

Reviewers: V.D., Australian National University; and K.D., University of St. Andrews.

The authors declare no conflict of interest.

Freely available online through the PNAS open access option.

[1]To whom correspondence may be addressed. Email: capasso@seas.harvard.edu or ginis@seas.harvard.edu.

This article contains supporting information online at www.pnas.org/lookup/suppl/doi:10.1073/pnas.1714953114/-/DCSupplemental.

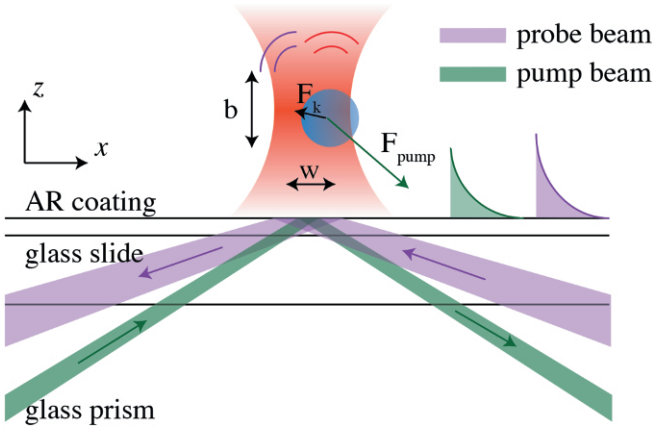

Fig. 1. The optically trapped microsphere in its anisotropic environment. The optical trap (660 nm, 12 mW) has a Rayleigh length, *b*, larger than the beam waist, *w*, resulting in a restoring force approximately 5 times stronger in the lateral direction. Additionally, near-wall hydrodynamic coupling results in anisotropic drag that is consistently larger in the vertical direction. As a result, the particle has a different response function in the two directions. The optical force of the pump beam has components in *z* and *x*. At a driving frequency between the two cutoff frequencies, the particle's response can have large phase differences between the two directions, generating elliptical orbits. F_k represents the restoring force of the trap. The dissipative drag and the stochastic force are not visualized. For a detailed description of the setup, see Fig. S1.

the Debye length in water (see *Height-Dependent Trap Spring Constant*).

In the absence of boundary effects, viscous drag, γ, is isotropic, given by Stokes' Law, $\gamma_0 = 6\pi\eta R$, where η is the viscosity of the fluid and R is the radius of a sphere. The presence of the boundary results in an anisotropic, height-dependent drag coefficient (40, 41). The predicted drag in the direction perpendicular to the surface (z) is always larger than that in the lateral direction (x) (see *Height-Dependent Damping Coefficient*). Due to the spherical symmetry of the particle, in low Reynolds number hydrodynamics ($\mathrm{Re} \ll 1$), we may assume that the drag forces parallel and perpendicular to a plane boundary are uncoupled, such that γ_{ij} is diagonal with unequal elements (42).

$\vec{B}(t)$ is the fluctuating thermal force due to collisions between the microparticle and molecules of the fluid. In each dimension, the fluctuations are expected to be uncorrelated, with $\langle B_i(t)\rangle = 0$, where $\tilde{B}(\omega)$ is spectrally flat. Its mean-squared magnitude is predicted by the fluctuation-dissipation theorem to be $\langle B_i(t)^2\rangle = 2\gamma_i k_B T$, where k_B is the Boltzmann constant. It is important to note that thermal noise increases not only with temperature but also with increased viscous drag and is the dominant source of noise in our system (18).

Lastly, the external force, which drives the periodic motion of the particle, is an optical force produced by the interaction of the microsphere with the evanescent field of a totally internally reflected TM-polarized plane wave. In the dipolar approximation, the interaction can be broadly understood to have two components: one proportional to the gradient of the field, which attracts the particle toward the surface, and the other proportional to the linear momentum of the wave, which pushes the particle along the surface (see *Optical Force on a Dipolar Particle in an Evanescent Field*).

For small, lossless particles ($\mathrm{Im}[\alpha] \ll \mathrm{Re}[\alpha]$), the optical force is predominantly oriented along the z direction. But as the particle increases in size, its interaction with the evanescent wave becomes more complex (43). In this regime, called the Mie regime, light is scattered into every direction in the xz plane. As a result, the direction of the net applied force is observed to rotate toward the horizontal direction. A detailed analysis of the forces acting on the particle in the Mie regime is shown in *Optical Force on a Mie Particle in an Evanescent Field*.

Microparticle Mechanical Response

The mechanical response of our microsphere to an applied force is frequency-dependent and can be found by solving Eq. **1**. We can neglect the particle's inertia while working at time scales much larger than the momentum relaxation time, $\tau_p = m^\star/\gamma$, which, in our system, is below 1 μs (44, 45). Inserting a time-harmonic solution, we then find that

$$\tilde{x}_i(\omega) = \chi_{ij}(\omega)\tilde{F}_j(\omega), \qquad [2]$$

in which we identified the mechanical susceptibility $\chi_{ij}(\omega)$ of the system as $\left(\chi^{-1}(\omega)\right)_{ij} = \kappa_{ij} + i\omega\gamma_{ij}$.

The motion is separable, with two different cutoff frequencies, $f_c = \kappa/2\pi\gamma$, in the x and z directions. Eq. **2** implies that though $F_x(t)$ and $F_z(t)$ may be in phase, as is the case with our optically driven system, $x(t)$ and $z(t)$ need not. The maximum phase lag between motion in the two directions is $\pi/2$, making it possible to induce elliptical trajectories of the particle. Furthermore, the linearity of the system ensures that Eq. **2** applies whether the force is random or periodic. Thus, in our case, where the external force on our particle is composed of both a driven and a stochastic component, the thermal motion of the microsphere may be considered separately from the time evolution of the particle's mean position.

Experiment

A schematic of the experiment is shown in Fig. 1 (also see Fig. S1 for details). All experiments are performed at room temperature in a water-filled, closed, 25-μm-deep microfluidic chamber. An antireflection (AR) coating is applied to the bottom glass–water interface of the chamber to eliminate standing-wave modulation of the trap laser beam (46). Each polystyrene microsphere is optically trapped by a focused CW laser beam (660-nm-wavelength) via a high numerical aperture (N.A. = 1.2) water-immersion objective. The vertical position of the focus, and consequently the height of the trapped bead, is adjusted using a piezo—by lifting and lowering the objective relative to the chamber. In addition to the trap beam, which enters the chamber from above, two lasers, both p-polarized, are incident from below at greater than critical angle ($\theta_c = 61.4°$): a low-power (<1 mW), 637-nm beam acts as the probe for the vertical (z) position of the particle (15, 47), and a second laser (785 nm, around 100 mW average power before modulation) generates the periodic optical force that pulls on the microparticle. The second beam, which we refer to as the pump beam, is modulated by a chopper set to a desired frequency. A detailed explanation of the analysis may be found in *Analysis Flow*.

Fig. 2 plots the predicted and observed 2D trajectories of a 2-μm PS microsphere under the influence of a periodic optical force. Predictions were made based on the optical force, mean trap stiffnesses, and bead radius fitted to experimental data. The measured trajectories are mean trajectories, extracted from 100-s measurements where each point is the averaged 2D position of the particle at a certain phase in the chopper actuation cycle. As the frequency of the modulation is increased, several distinct behaviors are observed that can be understood in relation to the cutoff frequencies in the two spatial directions.

Below both cutoff frequencies, the position of the particle is in phase with the applied force. In this case, the particle's motion in x and z is in phase with one another, and it undergoes linear oscillation with a direction determined primarily by the ratio of the trap stiffnesses κ_x/κ_z. In our case, the ratio is about 5. Above both cutoff frequencies, the motion is again linear as the oscillations are now out of phase with the applied force in both directions. However, the direction of motion is now determined

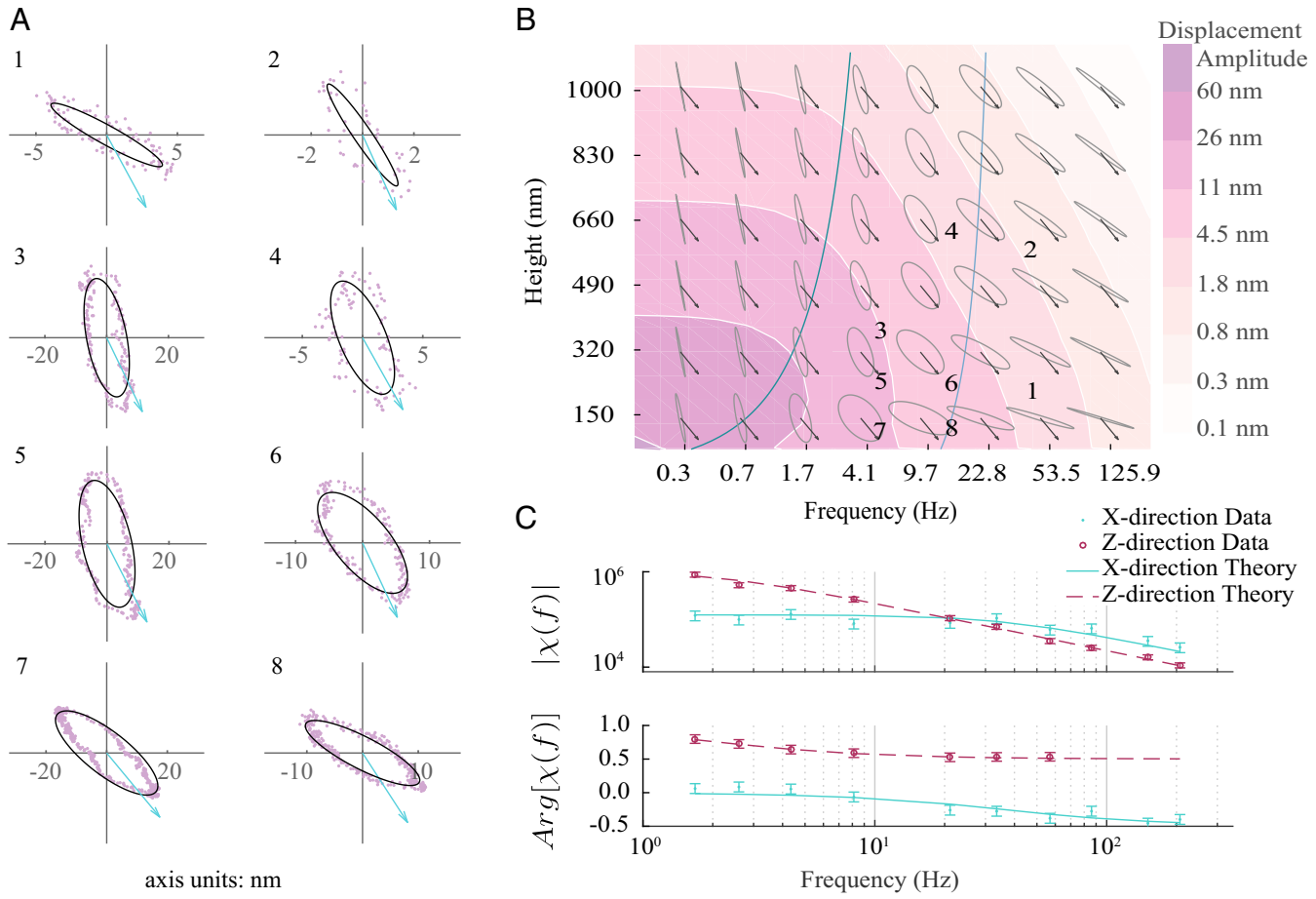

Fig. 2. (*A*) Predicted and measured 2D motion of a 1-μm-radius bead when driven by a periodic optical force from an evanescent field. The blue arrows indicate the direction of the optical force. Each tile in *A* corresponds to a particular height (z) and modulation frequency (ω_0) and is numbered corresponding to its location on the grid (*B*). The details of the measurement parameters are given in Table S1. (*B*) Grid of predicted particle trajectories where the horizontal axis represents the driving frequency and the vertical axis is the height above the surface. The displacement amplitude in nanometers is defined as the length of the semimajor axis of each orbit. Calculated cutoff frequencies in the x and z directions are drawn as blue lines. At all heights, the cutoff frequency in the z direction is lower than that in the x direction, due to a larger trap stiffness in the lateral direction. (*C*) Measured amplitude and phase of frequency-dependent mechanical susceptibility, $\chi(f)$, at a height of 400 nm, compared with predictions.

by the ratio of the damping coefficients γ_x/γ_z. As the particle nears the surface, γ_z diverges, while γ_x approaches a constant value, and the motion becomes more and more parallel to the wall. But between the two cutoff frequencies, the motions in the two spatial directions go out of phase with one another, and stable, elliptical orbits are established.

In Fig. 3 we compare our measurements against Mie theory predictions for a fixed modulation frequency. As the microparticle radius increases, the net optical force from the evanescent field increases for a given field strength and configuration, and the direction of the force rotates slowly toward the horizontal. In addition, since hindered diffusion theory predicts drag near a surface to increase as a function of the ratio z/R, where z is the separation and R is the radius, increasing the radius has similar effects as decreasing separation. Therefore, large beads tend to move parallel to the surface, regardless of their direction of excitation.

The Evanescent Wave Technique as a Method of Angular Momentum Generation

The observed phenomenon may find application as an efficient generator of small-radius orbital motion. While we do not suggest that this method supplants the study and use of structured light beams in colloidal systems, here we provide a detailed quantitative comparison and discuss the distinguishing features of our system.

One manner of quantifying angular motion is to consider the torque applied by the particle to the fluid, $\tau_{app}(t) = \vec{r}(t) \times \gamma \vec{v}(t)$, where γ is the tensor described in Eq. **1**. For a particle undergoing steady-state, elliptical motion in fluid, this quantity is on average the same as the torque applied to the particle. Fig. 4 shows τ_{app} accumulating over 100 s for a bead driven at two different frequencies, which agree well with predictions. Another method of quantifying this angular motion is to calculate the constant, nonzero intrinsic orbital angular momentum in the steady state, given by $\langle L_{in} \rangle = \omega |\tilde{x}||\tilde{z}| \sin(\phi_z - \phi_x)$, where ϕ_x and ϕ_z are the phases of the complex mechanical susceptibilities χ_x and χ_z in the x and z directions, respectively, and $\langle L_{in} \rangle$ is normalized by mass (see *Angular Momentum Analysis*). This quantity is useful in allowing direct comparison with existing reports in literature, where we do not have access to values of the damping parameter, γ, but can estimate velocity and orbital radius. In our unoptimized set-up, the largest L_{in} was measured to be $4.9 \times 10^{-15} \mathrm{m}^2/\mathrm{s}$, where $\phi_z - \phi_x$ was closest to $\pi/2$. The configuration for this measurement was a 2-μm-diameter bead driven at 4.6 Hz at a separation of around 200 nm from the surface (corresponding to point 5 in Fig. 2). In comparing this value with previous reports for dielectric particles driven by structured light,

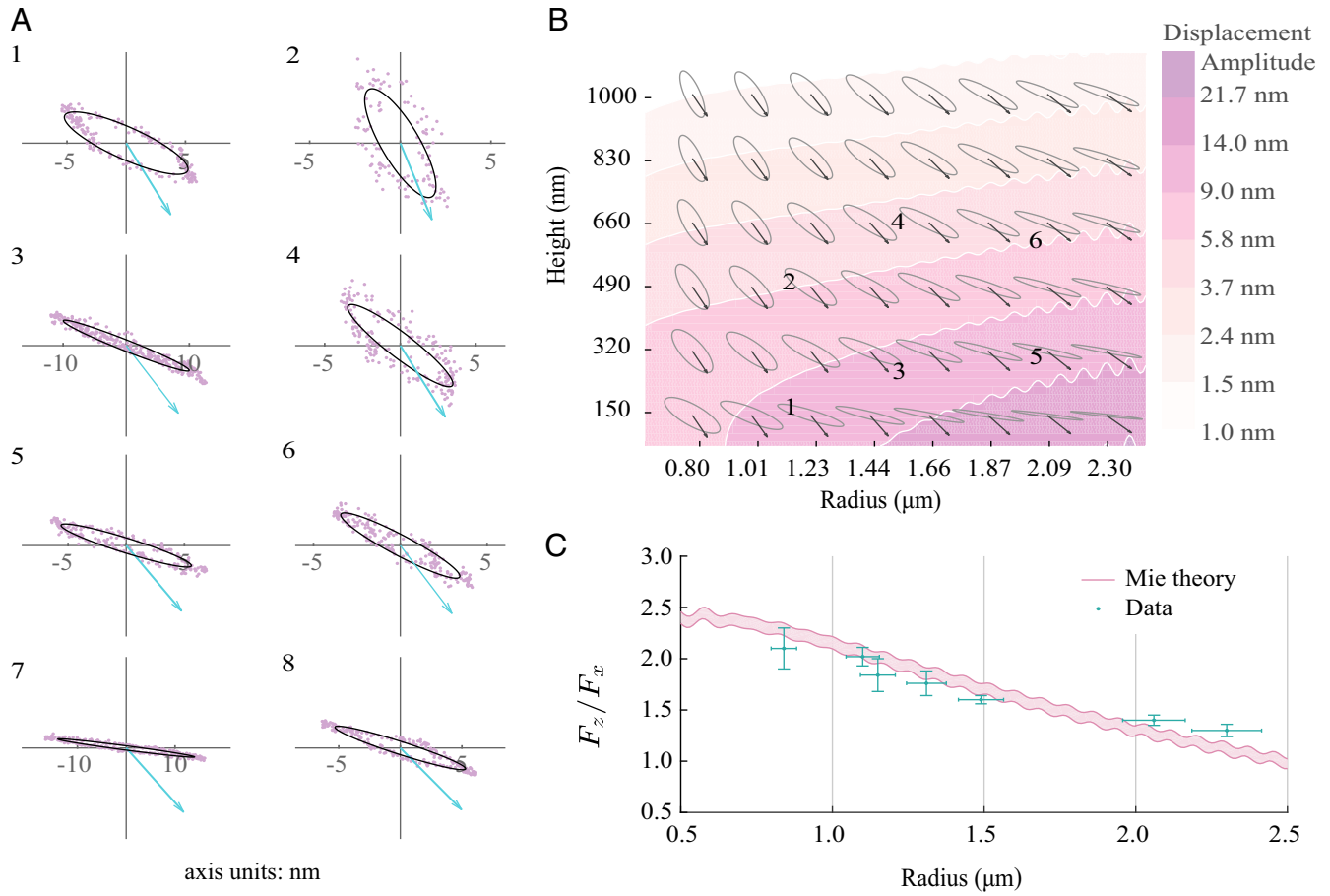

Fig. 3. (*A*) Predicted and measured motion of 0.6- to 2.5-μm-radius beads when driven by a periodic optical force from an evanescent field that is switched on and off at 20 Hz. The blue arrows indicate the direction of the optical force. Each tile in *A* corresponds to a particular height and bead radius and is numbered corresponding to its location on the grid (*B*). The details of the measurement parameters are given in Table S2. (*B*) Grid of predicted particle trajectories based on Mie theory calculations, where the horizontal axis represents bead radius and the vertical axis is the height above the surface. The displacement amplitude in nanometers is defined as the length of the semimajor axis of each orbit. The trajectories labeled 7 and 8 are for a 2.85-μm-radius bead, outside the scope of our Mie theory calculations. (*C*) Ratio of measured optical forces in the *z* and *x* directions compared with Mie theory. Shaded area shows the uncertainty in the microsphere index of refraction ($n = 1.575 \pm 0.005$). Generally, as microparticle radius increases, the direction of the optical force rotates toward the horizontal.

such as by optical vortices (30–33), we find our value comparable when normalized by laser power. With optimization of driving frequency and bead radius or changes in the power or wavelength of the pump beam, further gains may be expected. For details regarding this calculation, see *Angular Momentum Analysis* and *Comparing the Generation of Angular Momentum with Common Existing Techniques*.

It is relevant, at this point, to bring up another body of previous work on the orbital motion of colloids, distinct from structured light studies. One specific scheme involves a particle positioned in between a pair of misaligned beams (48). It is a part of a general class of studies in which particles are observed to undergo circulation while immersed in a static force field with nonzero curl (25, 49). In addition, Angelsky et al. observed orbital angular momentum transfer in circularly polarized Gaussian beams as a manifestation of the macroscopic "spin energy flow," thus confirming the theory of inhomogeneously polarized paraxial beams (34, 50).

We are careful to distinguish the nature of the orbital motion described in our current report from this class of studies. The motion observed in our work is not fully determined by a particle's passive interaction with a static optical force field but rather by a periodically driven microsphere's mechanical response. Since our system exhibits driven rather than passive motion, an array of such trapped particles can be made to move in phase, enabling unique collective behaviors that are thus far unexplored.

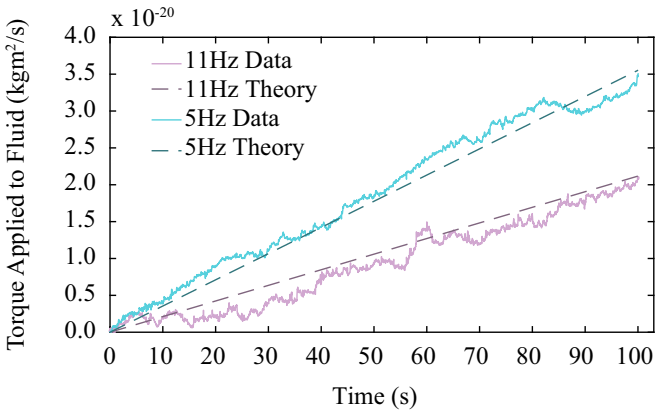

Fig. 4. Measured and predicted torque applied to fluid integrated over time for a 2-μm PS bead driven at 11 Hz and 5 Hz frequency at a height of about 200 nm, corresponding to points 5 and 6 in Fig. 2. The force on the bead is the same in both curves.

In addition, while a particle or a collection of particles may be easily made to orbit in a plane parallel to a nearby surface using existing techniques, methods for obtaining orbits in a plane perpendicular to such a surface are less readily available. Particularly in on-chip geometries where space may be an issue, our method of actuation may provide a useful alternative.

Finally, since the motion observed in our work is actively controlled, main parameters of orbital motion—such as rotational rate and radius—are decoupled and can be independently tuned. For instance, to increase the orbital radius in our experiment without affecting the rotation rate, one can simply raise the pump beam's intensity without changing its modulation frequency. It should be noted, however, that in our scheme the maximum radius of rotation cannot exceed the limits of the optical trap. If complete flexibility in orbital radii is desired, structured light approaches are more suitable. Additionally, if the goal is near-circular motion, a nearby surface or some other symmetry-breaking element is required, making the work described here potentially unsuitable for manipulation in bulk fluid or in vacuum. Also, larger radii of rotation can be achieved in general by the use of structured light, as the requirement that a particle remains in a single-beam Gaussian harmonic trap may prove too limiting for certain applications.

Thus, our technique can be considered as complementary to existing methods for generating orbital angular momentum, rather than substitutive. The ideas underlying both can be combined to extend the parameter range of orbital angular momentum generation in microparticles using optical forces.

Conclusion

Using a highly sensitive detection scheme, we investigated the dynamics of trapped microspheres under the influence of a temporally modulated force. We find good agreement between our model and the measured motion validating our method of generating elliptical orbits with sustained nonzero orbital angular momentum.

ACKNOWLEDGMENTS. We thank the groups of Evelyn Hu and David Weitz at Harvard University for shared equipment and laboratory access. All fabrication was done in the Harvard Center for Nanoscale Sciences (CNS) clean room facility. We acknowledge the support of NSF GFRP Grant DGE1144152 and Research Foundation Flanders Grant 12O9115N.

1. Wang K, Schonbrun E, Steinvurzel P, Crozier KB (2011) Trapping and rotating nanoparticles using a plasmonic nano-tweezer with an integrated heat sink. *Nat Commun* 2:469.
2. Righini M, Volpe G, Girard C, Petrov D, Quidant R (2008) Surface plasmon optical tweezers: Tunable optical manipulation in the femtonewton range. *Phys Rev Lett* 100:8–11.
3. Min C, et al. (2013) Focused plasmonic trapping of metallic particles. *Nat Commun* 4:2891.
4. Wang K, Schonbrun E, Crozier KB (2009) Propulsion of gold nanoparticles with surface plasmon polaritons: Evidence of enhanced optical force from near-field coupling between gold particle and gold film. *Nano Lett* 9:2623–2629.
5. Grigorenko A, Roberts N, Dickinson M, Zhang Y (2008) Nanometric optical tweezers based on nanostructured substrates. *Nat Photon* 2:365–370.
6. Povinelli ML, et al. (2005) Evanescent-wave bonding between optical waveguides. *Opt Lett* 30:3042–3044.
7. Volpe G, Quidant R, Badenes G, Petrov D (2006) Surface plasmon radiation forces. *Phys Rev Lett* 96:238101.
8. Woolf D, Kats MA, Capasso F (2014) Spoof surface plasmon waveguide forces. *Opt Lett* 39:517–520.
9. Bliokh KY, Bekshaev AY, Nori F (2013) Extraordinary momentum and spin in evanescent waves. *Nat Commun* 5:14.
10. Wang SB, Chan CT (2014) Lateral optical force on chiral particles near a surface. *Nat Commun* 5:1–8.
11. Rodríguez-Fortuño FJ, Engheta N, Martínez A, Zayats AV (2015) Lateral forces on circularly polarizable particles near a surface. *Nat Commun* 6:8799, and erratum (2015) 6:10263.
12. Hayat A, Mueller JPB, Capasso F (2015) Lateral chirality-sorting optical forces. *Proc Natl Acad Sci USA* 112:13190–13194.
13. Grier DG (2003) A revolution in optical manipulation. *Nature* 424:810–816.
14. Neuman KC, Block SM (2004) Optical trapping. *Rev Sci Instrum* 75:2787–2809.
15. Prieve DC, Bike SG, Frej NA (1990) Brownian motion of a single microscopic sphere in a colloidal force field. *Faraday Discuss Chem Soc* 90:209–222.
16. Florin EL, Pralle A, Hörber JH, Stelzer EH (1997) Photonic force microscope based on optical tweezers and two-photon excitation for biological applications. *J Struct Biol* 119:202–211.
17. Geraci AA, Papp SB, Kitching J (2010) Short-range force detection using optically cooled levitated microspheres. *Phys Rev Lett* 105:101101.
18. Liu L, Kheifets S, Ginis V, Capasso F (2016) Subfemtonewton force spectroscopy at the thermal limit in liquids. *Phys Rev Lett* 116:228001.
19. Leach J, Mushfique H, di Leonardo R, Padgett M, Cooper J (2006) An optically driven pump for microfluidics. *Lab A Chip* 6:735–739.
20. Terray A, Oakey J, Marr DWM (2002) Microfluidic control using colloidal devices. *Science* 296:1841–1844.
21. MacDonald M, Spalding G, Dholakia K (2003) Microfluidic sorting in an optical lattice. *Nature* 426:421–424.
22. Lutz C, Kollmann M, Bechinger C (2004) Single-file diffusion of colloids in one-dimensional channels. *Phys Rev Lett* 93:026001.
23. Garces-Chavez V, et al. (2006) Extended organization of colloidal microparticles by surface plasmon polariton excitation. *Phys Rev B* 73:085417.
24. Jonas A, Zemanek P, Florin EL (2001) Single-beam trapping in front of reflective surfaces. *Opt Lett* 26:1466–1468.
25. Roichman Y, Sun B, Stolarski A, Grier DG (2008) Influence of nonconservative optical forces on the dynamics of optically trapped colloidal spheres: The fountain of probability. *Phys Rev Lett* 101:1–5.
26. Wang S, Chan CT (2016) Strong optical force acting on a dipolar particle over a multilayer substrate. *Opt Express* 24:2235–2241.
27. Salary MM, Mosallaei H (2016) Strong optical force acting on a dipolar particle over a multilayer substrate. *Phys Rev B* 24:2235–2241.
28. Bekshaev AY, Bliokh KY, Nori F (2013) Mie scattering and optical forces from evanescent fields: A complex-angle approach. *Opt Express* 21:7082–7095.
29. Yang Y, Zang WP, Zhao ZY, Tian JG (2012) Optical forces on Mie particles in an airy evanescent field. *Opt Express* 20:25681–25692.
30. O'neil A, MacVicar I, Allen L, Padgett M (2002) Intrinsic and extrinsic nature of the orbital angular momentum of a light beam. *Phys Rev Lett* 88:053601.
31. Volke-Sepulveda K, Garces-Chavez V, Chavez-Cerda S, Arlt J, Dholakia K (2002) Orbital angular momentum of a high-order Bessel light beam. *J Opt B Quantum Semiclassical Opt* 4:S82.
32. Garces-Chavez V, et al. (2003) Observation of the transfer of the local angular momentum density of a multiringed light beam to an optically trapped particle. *Phys Rev Lett* 91:093602.
33. Loxpez-Mariscal C, Gutierrez-Vega JC, Milne G, Dholakia K (2006) Orbital angular momentum transfer in helical Mathieu beams. *Opt Express* 14:4182–4187.
34. Angelsky OV, et al. (2012) Circular motion of particles suspended in a Gaussian beam with circular polarization validates the spin part of the internal energy flow. *Opt Express* 20:11351–11356.
35. Angelsky OV, et al. (2012) Orbital rotation without orbital angular momentum: Mechanical action of the spin part of the internal energy flow in light beams. *Opt Express* 20:3563–3571.
36. Xiao G, Yang K, Luo H, Chen X, Xiong W (2016) Orbital rotation of trapped particle in a transversely misaligned dual-fiber optical trap. *IEEE Photon J* 8:1–8.
37. Uhlenbeck GE, Ornstein LS (1930) On the theory of the Brownian motion. *Phys Rev* 36:823–841.
38. Berg-Sorensen K, Flyvbjerg H (2004) Power spectrum analysis for optical tweezers. *Rev Sci Instrum* 75:594–612.
39. Nieminen TA, et al. (2014) Optical tweezers: Theory and modelling. *J Quant Spectrosc Radiat Transf* 146:59–80.
40. Brenner H (1961) The slow motion of a sphere through a viscous fluid towards a plane surface. *Chem Eng Sci* 16:242–251.
41. Goldman A, Cox RG, Brenner H (1967) Slow viscous motion of a sphere parallel to a plane wall i: Motion through a quiescent fluid. *Chem Eng Sci* 22:637–651.
42. Nägele G (1996) On the dynamics and structure of charge-stabilized suspensions. *Phys Rep* 272:215–372.
43. Almaas E, Brevik I (1995) Radiation forces on a micrometer-sized sphere in an evanescent field. *J Opt Soc Am B* 12:2429–2438.
44. Huang R, et al. (2011) Direct observation of the full transition from ballistic to diffusive Brownian motion in a liquid. *Nat Phys* 7:576–580.
45. Kheifets S, Simha A, Melin K, Li T, Raizen MG (2014) Observation of Brownian motion in liquids at short times: Instantaneous velocity and memory loss. *Science* 343:1493–1496.
46. Liu L, Woolf A, Rodriguez AW, Capasso F (2014) Absolute position total internal reflection microscopy with an optical tweezer. *Proc Natl Acad Sci USA* 111:E5609–E5615.
47. Prieve DC, Walz JY (1993) Scattering of an evanescent surface wave by a microscopic dielectric sphere. *Appl Opt* 32:1629–1641.
48. Xiao G, Yang K, Luo H, Chen X, Xiong W (2016) Orbital rotation of trapped particle in a transversely misaligned dual-fiber optical trap. *IEEE Photon J* 8:1–8.
49. Pesce G, Volpe G, De Luca AC, Rusciano G, Volpe G (2009) Quantitative assessment of non-conservative radiation forces in an optical trap. *Europhys Lett* 86:38002.
50. Bekshaev A, Bliokh KY, Soskin M (2011) Internal flows and energy circulation in light beams. *J Opt* 13:053001.